



**HAL**  
open science

## Self and N<sub>2</sub> broadening coefficients of H<sub>2</sub>S probed by submillimeter spectroscopy: Comparison with IR measurements and semi-classical calculations

Meriem Mouelhi, A. Cuisset, C. Jellali, S. Galalou, H. Aroui, Robin Bocquet, Gaël Mouret, F. Rohart, Francis Hindle

### ► To cite this version:

Meriem Mouelhi, A. Cuisset, C. Jellali, S. Galalou, H. Aroui, et al.. Self and N<sub>2</sub> broadening coefficients of H<sub>2</sub>S probed by submillimeter spectroscopy: Comparison with IR measurements and semi-classical calculations. *Journal of Quantitative Spectroscopy and Radiative Transfer*, 2020, 247, pp.106955. 10.1016/j.jqsrt.2020.106955 . hal-03489669

**HAL Id: hal-03489669**

<https://hal.science/hal-03489669v1>

Submitted on 20 May 2022

**HAL** is a multi-disciplinary open access archive for the deposit and dissemination of scientific research documents, whether they are published or not. The documents may come from teaching and research institutions in France or abroad, or from public or private research centers.

L'archive ouverte pluridisciplinaire **HAL**, est destinée au dépôt et à la diffusion de documents scientifiques de niveau recherche, publiés ou non, émanant des établissements d'enseignement et de recherche français ou étrangers, des laboratoires publics ou privés.



Distributed under a Creative Commons Attribution - NonCommercial 4.0 International License

# **Self and N<sub>2</sub> broadening coefficients of H<sub>2</sub>S probed by submillimeter spectroscopy: comparison with IR measurements and semi-classical calculations.**

**M. Mouelhi <sup>a,b</sup>, A. Cuisset <sup>a\*</sup>, F. Hindle <sup>a</sup>, C. Jellali <sup>b</sup>, S. Galalou <sup>b</sup>, H. Aroui <sup>b</sup>, R. Bocquet <sup>a</sup>, G. Mouret <sup>a</sup> and F. Rohart <sup>c</sup>**

<sup>a</sup> *Laboratoire de Physico-Chimie de l'Atmosphère EA 4493, Université du Littoral Côte d'Opale, 189A Avenue Schumann, 59140 Dunkerque, France*

<sup>b</sup> *Université de Tunis, Laboratoire de Spectroscopie et Dynamique Moléculaire, Ecole Nationale Supérieure d'Ingénieurs de Tunis, 5 Av Taha Hussein 1008 Tunis, Tunisia.*

<sup>c</sup> *University of Lille, CNRS, UMR 8523 – PhLAM - Physique des Lasers, Atomes et Molécules, F-59000 Lille, France.*

\*Corresponding author:

Arnaud Cuisset

Phone: 33 (0)3 28 23 76 13

Fax : 33 (0)3 28 65 82 44

Email : [arnaud.cuisset@univ-littoral.fr](mailto:arnaud.cuisset@univ-littoral.fr)

## ABSTRACT

High-resolution lines of H<sub>2</sub>S self-perturbed and perturbed by N<sub>2</sub> have been recorded at room temperature using a frequency modulated THz spectrometer at pressures of H<sub>2</sub>S ranging from 0.1 to 1.0 mbar. A non-linear least squares fitting of these spectra has been performed to retrieve self- and N<sub>2</sub>-broadening coefficients of pure rotational transitions (mainly in the <sup>R</sup>Q sub-branch) of H<sub>2</sub>S in the submillimeter region. We show that the lineshapes are well reproduced by the Speed-Dependent Voigt profile accounting for the speed dependence of relaxation rates which display linear pressure dependencies. Using the Robert and Bonamy formalism, these coefficients were calculated, showing the need to account for all contributions of the intermolecular interaction for N<sub>2</sub>- broadening. The calculated coefficients are consistent with the measured data and the average accuracy of the line parameters has been estimated to be about 5 %. The observed  $J''$  and  $K_a''$  rotational dependences have been analyzed using an empirical model and compared to previous rovibrational studies in the  $\nu_2$  fundamental band. In our study the self- and the N<sub>2</sub>- broadening coefficients decreases monotonically with  $K_a''$  and  $J''$ , respectively.

### Key words:

Broadening coefficient, H<sub>2</sub>S, submillimeter-wave spectroscopy, speed-dependence effects, semi-classical calculation, rotational dependencies.

## 1. Introduction

With its characteristic foul odor of rotten eggs, hydrogen sulfide ( $\text{H}_2\text{S}$ ) is a colorless, highly toxic, corrosive, and flammable gas, soluble in various liquids including water and alcohol. Most of the atmospheric  $\text{H}_2\text{S}$  has natural origins. It is often produced from the microbial breakdown of organic matter in the absence of oxygen gas via anaerobic digestion. Therefore,  $\text{H}_2\text{S}$  is a good marker of the food spoilage especially fish [1]. Moreover,  $\text{H}_2\text{S}$  is one of the main trace gases released from volcanoes and the emission ratio  $\text{H}_2\text{S}:\text{SO}_2$  is an important geochemical probe. Some satellite instruments such as the Infrared Atmospheric Sounding Interferometer (IASI)/MetOp have observed large  $\text{H}_2\text{S}$  plumes during explosive volcanic events [2].  $\text{H}_2\text{S}$  is detected **not** only in the Earth's atmosphere but also in the atmospheres of Jupiter [3] and of the ice giants Neptune and Uranus with the Gemini-North/NIFS H-band observations [4]. Finally, due to its high toxicity and its very weak value of the low permissible concentration level which is equal to  $0.008 \text{ mg/m}^3$ , the monitoring of anthropogenic  $\text{H}_2\text{S}$  in industrial and urban atmospheres is very challenging. Continuous sensing has been performed by Raman lidar [5]. Contrary to  $\text{SO}_2$ , IR measurements of  $\text{H}_2\text{S}$  are sparse and difficult [2] and an accurate monitoring of atmospheric  $\text{H}_2\text{S}$  at trace levels requires to fit the  $\text{H}_2\text{S}$  atmospheric spectra with the best set of spectroscopic parameters and the most appropriate line profiles.

From a spectroscopic point of view,  $\text{H}_2\text{S}$  is similar to  $\text{H}_2\text{O}$  and represents a very light asymmetric top with a Ray parameter equal to 0.5234 [6]. Due to its large asymmetry, the rotational spectrum of  $\text{H}_2\text{S}$  shows no coherent line pattern. At room temperature, intense rotational lines are spread out over the complete submillimetre (smm)-wave regions. Numerous investigations have been performed on the pure rotational spectrum of  $\text{H}_2\text{S}$ ; most of them deal with line frequency analyses from the micro-wave (mw) [8] to the far-IR regions [7]. Ground state (GS) smm rotational line profile analyses and broadening parameter measurements are almost non-existent except the study of Helminger and De Lucia **who** determine the self-broadening parameters for only four rotational transitions of  $\text{H}_2\text{S}$  [8]. The temperature dependences of these parameters were studied by **Ball *et al.*** in 1999 [9]. However, the ability of frequency-modulated rotational spectroscopy to perform quantitative analysis of gas phase molecular constituents has been demonstrated [10] and a systematic study of the broadening parameters and their rotational dependences is now possible even for asymmetric top molecules [11]. Most of the broadening parameters of  $\text{H}_2\text{S}$  have been measured in the IR region from rovibrational transitions belonging to fundamental and combination vibrational bands. Tan *et al.* [12] have collected for **HITRAN-2016** all the experimental self and air-broadening parameters of  $\text{H}_2\text{S}$  provided from different experimental IR studies [13-17]. A large variability of the IR data

is observed and the vibrational dependence of the broadening parameters was neglected. Linear functions were used to describe the rotational dependences with a trend of the H<sub>2</sub>S self- and air-broadening parameters to decrease with  $J''+0.2K_a''$ . For all these studies, Voigt line-shapes have been used to fit the measured line profiles. Yet a recent extended analysis of the high resolution FTIR spectra of H<sub>2</sub>S in the region of the  $\nu_2$  bending fundamental band demonstrates that the line-shape fit could be significantly improved using the Hartman-Tran profile [18] with extra parameters taking into account the speed dependence of the relaxation. The half-widths analysis was made on the basis of the multi-spectrum fit procedure and the self-broadening coefficients were estimated for a few tens of lines for the three most abundant isotopologues [19].

In this study, we report the first measurements of self- and N<sub>2</sub>-broadening coefficients of H<sub>2</sub>S rotational lines for various values of the rotational quantum numbers  $J''$  and  $K_a''$  in a large frequency range mainly in the Q branch with a frequency-multiplication chain. Owing to the high signal-to-noise ratio (SNR) achieved using the frequency modulation technics, speed-dependence effects were systematically included in the fitting procedure of the observed lines. In addition, semi-classical calculations using the Robert-Bonamy (RB) formalism have been performed to predict the broadening parameters. The experimental smm broadening parameters are compared to previous IR measurements and to the semi-classical calculations. A new insight of the rotational dependence of the self- and N<sub>2</sub>-broadening is finally provided.

## 2. Experimental details and fitting methods

### 2.1. Experimental setup and experimental conditions

Self and N<sub>2</sub>-broadened H<sub>2</sub>S lines were recorded in the 160-850 GHz range using a frequency modulated smm-wave spectrometer. This spectrometer is composed by a frequency synthesizer operating in the range of 7-12 GHz and frequency referenced to a GPS timing signal. The microwave synthesizer is used to drive a frequency multiplication chain (Virginia diodes) covering 70 to 900 GHz as described previously [20]. A frequency modulation (FM) was applied to the synthesizer. The FM was fixed at 13 kHz with a modulation depth  $m$  selected for each line in the range (0.3-4.5 MHz) according to the expected linewidth, see Fig. 1. Observed lineshapes were recorded using an *InSb* liquid He-cooled bolometer from QMC instrument up to 330 GHz and a zero bias Schottky detector at higher frequencies. Corresponding signals were demodulated thanks to a lock-in amplifier operating at a twice the modulation frequency. The data acquisition and operation of the smm spectrometer was computer controlled using a dedicated program. The

gases H<sub>2</sub>S and N<sub>2</sub> were introduced into an absorption cell with Teflon windows presenting a clear diameter of 56 mm. Cell lengths, 28 cm and 113 cm, were employed depending on the observed line strengths. The spectrometer is located in a temperature controlled (295±1 K) room. The H<sub>2</sub>S and N<sub>2</sub> gases were purchased from Sigma Aldrich and Praxair respectively with claimed purities better than 99.5%. The gas pressures were measured with a vacuum gauge (Pfeiffer company, model CMR364) operating from 10<sup>-3</sup> to 1.1 mbar with a reading accuracy of 0.2%.

For self-broadening measurement, H<sub>2</sub>S pressures were chosen between 0.09 and 0.8 mbar. In the example spectrum shown in Fig. 1, the targeted frequency was swept using 50 kHz frequency steps of 300 ms duration, with a 100 ms time constant of the lock-in amplifier. Such conditions ensure negligible consequences of a limited detection bandwidth on observed lineshapes [21, 22].

To measure the N<sub>2</sub>-broadening coefficients, the rotational lines were recorded using the following procedure: the cell was first filled with pure H<sub>2</sub>S at a fixed pressure about 0.1 mbar then about 6-8 lineshapes were recorded with increased N<sub>2</sub> pressures up to about 0.8 mbar.

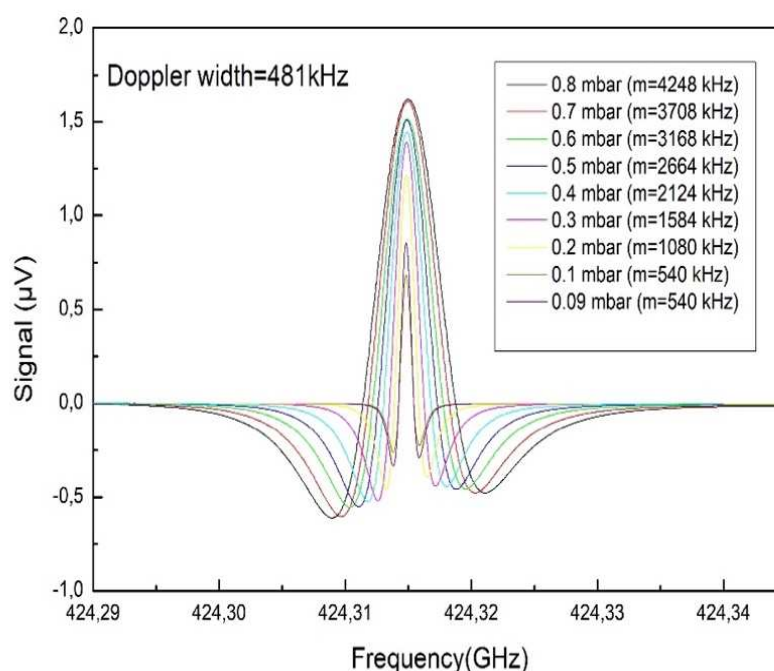


**Fig. 1:**  $4_{4,0} \leftarrow 4_{3,1}$  rotational line of pure H<sub>2</sub>S recorded at 424.315 GHz at different pressures. The modulation depth  $m$  is adjusted according to the estimated line width.

## 2.2 . Frequency-modulation submillimeter spectra

In case of a frequency modulated spectrometer with a lock-in detection operating at twice the modulation frequency  $\nu_m$ , the line profile  $F(\nu)$  has a W-shape which is given by the real part of the Fourier transform of [23]:

$$F(\nu) = \Re \left\{ 2 \int_0^{\infty} \Phi(t) \cdot J_2 \left[ 2\pi m t \cdot \text{sinc}(\pi \nu_m t) \right] \cdot \cos(2\pi \nu_m t) \cdot \exp(-2i\pi \nu t) \cdot dt \right\} \quad (1)$$

where  $\nu$  is the electromagnetic field frequency,  $J_2(x)$  is the 2<sup>nd</sup> order Bessel function,  $m$  is the modulation depth and  $\Phi(t)$  is the molecular polarization correlation function, that is the gas pulse response which is null for  $t < 0$ .

Let us first consider the usual Voigt profil  $F_V(\nu)$  which considers molecular displacements and molecular collisions as uncorrelated processes. It is simply given by the convolution of a Gaussian profile, related to the Doppler effect, and of a Lorentzian profile, related to collisional relaxation. So, its correlation function  $\Phi_V(t)$  is given by [23]:

$$\Phi_V(t) = \exp \left[ 2i\pi \nu_0 t - 2\pi \Gamma_{0,V} t - \left( \frac{k \nu_{a0} t}{2} \right)^2 \right] \quad (2)$$

where  $\nu_0$  is the absorber line center frequency,  $\Gamma_{0,V}$  is the collisional broadening,  $k=2\pi\nu_0/c$  is the wavenumber with  $c$  the speed of light, and  $\nu_{a0} = \sqrt{\frac{2k_B T}{m_a}}$  is the most probable value of the absorber speed defined by the Boltzmann constant  $k_B$ , the temperature  $T$  and molecular mass  $m_a$  of the absorber.

Due to the large intensities of H<sub>2</sub>S rotational lines, the Beer-Lambert law had to be considered. This was done in the following way [24, 25]. The transmission of the gas  $T(\nu)$  is given by:

$$T(\nu) = \exp[-SP_a l F(\nu)] \quad (3)$$

where  $S$  is the line intensity,  $P_a$  is the absorbing gas partial pressure, and  $l$  the cell length. So, the pulse response  $\theta(t)$  of the whole sample is given by:

$$\text{for } t \geq 0: \theta(t) = \int_{-\infty}^{+\infty} T(\nu) \cdot \exp(+2i\pi \nu t) \cdot d\nu \quad (4a)$$

$$\text{for } t < 0: \theta(t) = 0 \quad (4b)$$

In the case of frequency modulation with a  $2f$ -detection, the detected signal  $D(\nu)$  is simply proportional to the real part of the Fourier transform:

$$D(\nu) \propto \Re \left\{ 2 \int_0^{\infty} \Theta(t) \cdot J_2 \left[ 2\pi m t \cdot \text{sinc}(\pi \nu_m t) \right] \cdot \cos(2\pi \nu_m t) \cdot \exp(-2i\pi \nu t) \cdot dt \right\} \quad (5)$$

Since such a frequency modulated spectrometer does not allow to measure absolute transmissions, line intensities were fixed at the theoretical values given by HITRAN [26]. Whereas ignoring the Beer-Lambert law leads to strongly erroneous relaxation rates, this approach remains quite reliable since a 25% error in line intensities leads to 1% deviation in retrieved relaxation parameters [25]. Note that the line profile detected by a frequency modulation spectrometer generally exhibits an asymmetry. This artifact may originate from baseline distortion and/or from the gas refractive index through residual standing waves [23]. It was taken into account by introducing an adjustable dispersion term chosen as proportional to the imaginary part of the Fourier transform of Eq. (5).

In a preliminary step to the fitting procedure, the baseline perturbations caused by the instability of the mm-wave optical alignment in the cell are modeled with a 3<sup>rd</sup> order polynomial function. Next the measured lines with corrected baseline are adjusted using a nonlinear least squares code based on the Eqs. (1-5). Signal amplitude, line center frequency, collisional parameters, as well dispersion term amplitude could be adjusted, whereas Doppler width, line intensities, as well as modulation depth and frequency, were kept fixed at the values corresponding to experimental conditions and tabulated parameters [26]. An example is presented in the Fig. 2 for the  $4_{4,0} \leftarrow 4_{3,1}$  rotational line of pure H<sub>2</sub>S measured at 295K. Using the Voigt profile and thanks to the good SNR obtained ( $\cong 900$ ), one observes a remarkable difference between observed (orange curve) and fitted (black curve) profiles. Particularly, the observed profile has an amplitude greater than the fitted one and thus is narrower, the amplitude of the residual (black curve) is estimated to 3% of the line amplitude. Such a departure is characteristic of speed dependent and/or of Dicke narrowing effects [27].

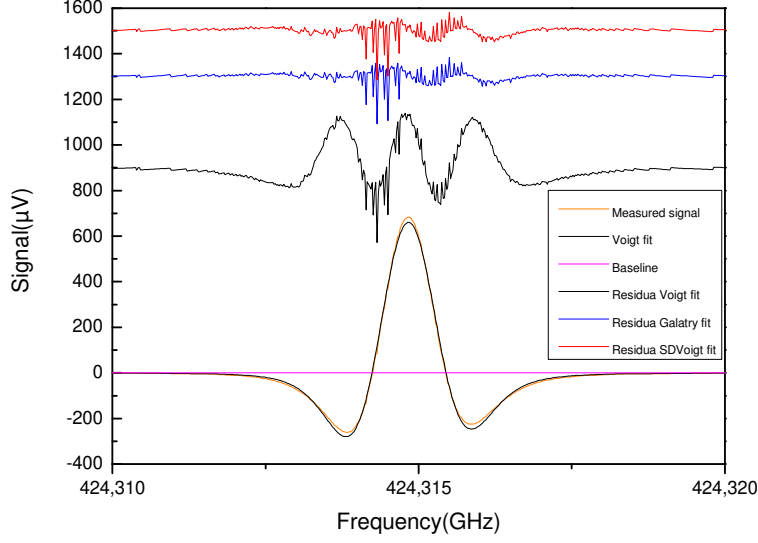


**Fig. 2:** Adjustments with Voigt, Galatry and SD-Voigt profiles and corresponding residuals enlarged by a factor of 10 for the  $4_{4,0} \leftarrow 4_{3,1}$  rotational line of pure  $\text{H}_2\text{S}$ . Experimental conditions:  $P=0.1$  mbar,  $T=295\text{K}$ , modulation depth  $m=540$  kHz, modulation frequency  $\nu_m=13$  kHz. Signal to noise ratio (SNR) is about 900. Doppler width= 482 kHz,  $\Gamma_{0,V}^{Exp}=397(20)$  kHz,  $\Gamma_{0,SDV}^{Exp}=469(10)$  kHz,  $\Gamma_{2,SDV}^{Exp}=100(4)$  kHz,  $\Gamma_{0,G}^{Exp}=446(20)$  kHz,  $B_G^{Exp}=315(10)$  kHz.

### 2.3. Speed-dependence effects

Departures from the Voigt profiles can be related to a combined influence of velocity changing collisions (Dicke narrowing) [28] and of the speed dependence of relaxation rates [29, 30]. To take into account these effects, the speed-dependent Galatry profile [31] has been retained because the corresponding correlation function has an analytical form, that is more convenient in case of frequency modulated absorption lines. Of course, this profile reduces to the usual Galatry profile [32] if SD-effects are negligible, or to the SD-Voigt profile [29, 30] if Dicke effect can be ignored.

Restricting to the velocity changing collisions only, the line narrowing can be modeled via the Galatry profile [32] whose correlation function is given by:

$$\Phi_G(t) = \exp \left\{ 2i\pi\nu_0 t - 2\pi\Gamma_{0,G}t + \frac{1}{2} \left( \frac{k\nu_{a0}}{2\pi B_G} \right)^2 [1 - 2\pi B_G t - \exp(-2\pi B_G t)] \right\} \quad (6)$$

In this equation  $B_G$  is the narrowing parameter that can be considered as the optical diffusion rate related to velocity changing collisions. Since this process influences the Doppler contribution,

the Galatry profile differs significantly from the Voigt profile in the Doppler regime, i.e. at low pressure, and coincide with the Voigt profile in the collisional regime.

Speed dependent effects can be considered separately by using the model first proposed by Berman [29] and Pickett [30] by assuming that collisional interaction is described by the empirical potential  $V(r) \propto r^{-q}$ , where  $r$  is the intermolecular distance and  $q$  an empirical parameter. This model leads to an hypergeometric dependence of the relaxation rate  $\Gamma_{SDV}(v_a)$  on the absorber speed  $v_a$ . However, this model requires rather long numerical calculations, so Rohart *et al.* [33] have proposed the quadratic approximation:

$$\Gamma_{SDV}(v_a) = \Gamma_{0,SDV} + \Gamma_{2,SDV} \cdot \left[ \left( \frac{v_a}{v_{a0}} \right)^2 - \frac{3}{2} \right] \quad (7)$$

which leads to a simpler correlation function:

$$\Phi_{SDV}(t) = \frac{\exp\left[2i\pi\nu_0 t - 2\pi\left(\Gamma_{0,SDV} - \frac{3}{2}\Gamma_{2,SDV}\right)t\right]}{(1+2\pi\Gamma_{2,SDV}t)^{3/2}} \cdot \exp\left[-\frac{(k\nu_{a0}t)^2}{4(1+2\pi\Gamma_{2,SDV}t)}\right] \quad (8)$$

where  $\Gamma_{0,SDV} = \left\langle \Gamma(v_a) \right\rangle_{v_a}$  is the mean relaxation rate over molecular speeds and  $\Gamma_{2,SDV}$  is a pressure dependent parameter describing the speed dependence of relaxation rates. Although approximate, this quadratic model has been retained for the extension of data bases to non Voigt spectral lineshapes [34]. Indeed, this model has been shown to be actually an accurate approximation of the hypergeometric one, at least for SNR lower than several thousand [35]. Moreover, it can be easily connected to the hypergeometric model via [36]

$$\frac{\Gamma_{2,SDV}}{\Gamma_{0,SDV}} = \frac{\lambda\mu}{3(1+\lambda)^{\mu/2}} \cdot M\left[1 - \frac{\mu}{2}; \frac{5}{2}; -\frac{3\lambda}{2}\right] \quad (9)$$

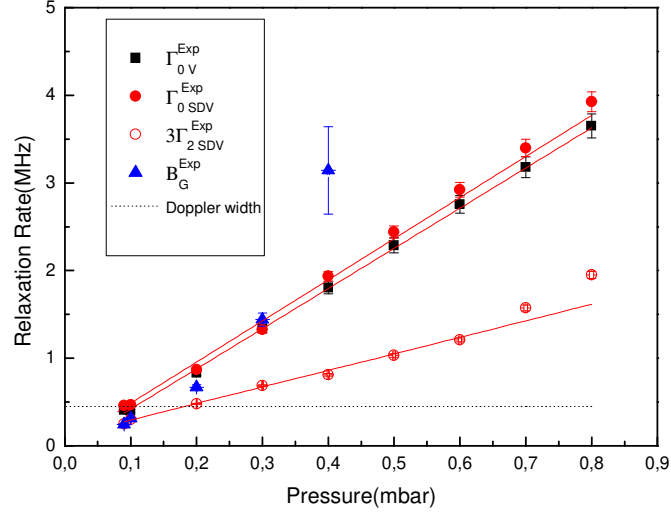
where  $\lambda = m_b/m_a$  is the mass ratio of buffer and absorbing molecules,  $\mu = (q-3)/(q-1)$ , and  $M[a;b;x]$  is the hypergeometric confluent function [37].

Let us consider the recorded H<sub>2</sub>S self-broadened lineshape displayed in Fig. 2 for a given pressure. One observes the quality of fits is similar using either the Galatry or the SD-Voigt profiles. For both cases and on account of the fairly good SNR obtained, one gets a nearly perfect adjustment with residuals significantly smaller than those obtained with the Voigt profile. Note this lineshape corresponds to the Doppler regime, the collisional broadening rate being lower than the Doppler broadening. However, at much higher pressures corresponding to the collisional

regime, and by contrast with the SD-Voigt profile, it was impossible to perform any fit using the Galatry profile. Let us consider the pressure dependences of the collisional relaxation rates  $\Gamma_{0,V}^{Exp}$ ,  $\Gamma_{0,SDV}^{Exp}$ ,  $\Gamma_{2,SDV}^{Exp}$ , as well as the Galatry optical diffusion rate  $B_G^{Exp}$ , as displayed on Fig. 3a. As expected for the binary collisional regime, Voigt and SD-Voigt relaxation rates behave linearly. On the contrary, the Galatry optical diffusion rate  $B_G^{Exp}$  exhibits a nonlinear pressure dependence for collisional broadenings larger than the Doppler width. Moreover,  $B_G^{Exp}$  could not be determined for pressures above 0.5 mbar, corresponding fits being impossible. This feature, well explained in Ref. [38], shows that observed departures from the Voigt profile are mainly due to the speed dependence of relaxation rates and that the Dicke effect has a negligible role and can be disregarded in case of self H<sub>2</sub>S relaxation. Similar difficulties were also encountered in the case of N<sub>2</sub>-induced relaxation of H<sub>2</sub>S, as displayed on Fig. 3b. In this case, the non-linear pressure dependence of  $B_G^{Exp}$  is also clearly evident, but occurs for pressures higher than in the pure H<sub>2</sub>S relaxation case (Fig. 3a), a feature due to the N<sub>2</sub>-H<sub>2</sub>S relaxation rate about twice smaller than the self H<sub>2</sub>S one, as explained in Ref. [38]. As a consequence, the role of velocity changing collisions has been disregarded and only the speed dependence of relaxation rates has been considered in the analysis of H<sub>2</sub>S collisional line shape.

The pressure dependence of the relaxation rate is obtained by linear least squares fittings as shown in Fig. 3a and Fig. 3b for the self-broadened  $4_{4,0} \leftarrow 4_{3,1}$  and the N<sub>2</sub>-broadened  $2_{2,1} \leftarrow 2_{1,2}$  transitions. The slopes of the straight lines gives the relaxation coefficients  $\gamma_{0,V}^{Exp}$ ,  $\gamma_{0,SDV}^{Exp}$  and  $\gamma_{2,SDV}^{Exp}$ , expressed in MHz/mbar and defined as  $\gamma_{0,V}^{Exp} = \frac{\partial \Gamma_{0,V}^{Exp}}{\partial P}$ ,  $\gamma_{0,SDV}^{Exp} = \frac{\partial \Gamma_{0,SDV}^{Exp}}{\partial P}$ ,  $\gamma_{2,SDV}^{Exp} = \frac{\partial \Gamma_{2,SDV}^{Exp}}{\partial P}$ , where  $\Gamma_{0,V}^{Exp}$  and  $\Gamma_{0,SDV}^{Exp}$  are the pressure broadenings,  $\Gamma_{2,SDV}^{Exp}$  is the relaxation speed dependence parameter and  $P$  is the gas pressure. The measured values of self-and N<sub>2</sub>-broadening coefficients  $\gamma_{0,V}^{Exp}$ ,  $\gamma_{0,SDV}^{Exp}$  and  $\gamma_{2,SDV}^{Exp}$  with their estimated uncertainties are listed in Tables 2 and 4, respectively.

**a**



**b**

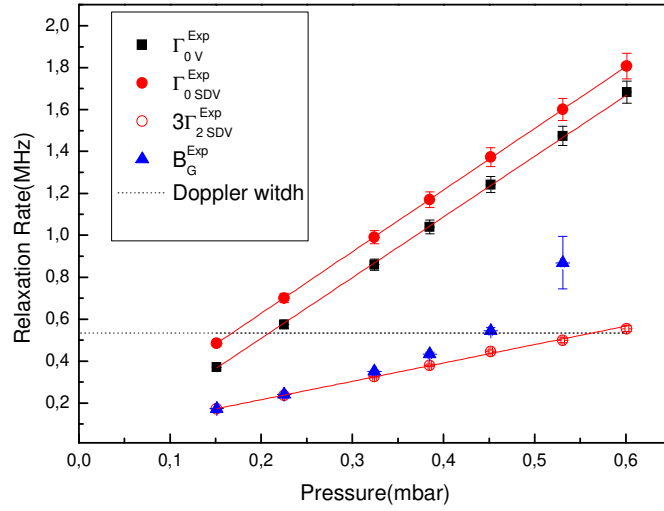


**Fig. 3:** Pressure dependence of the relaxation rates of H<sub>2</sub>S measured at room temperature ( $T = 295$  K). The relaxation coefficients are derived from weighted linear least squares:

(a) Self-broadened  $4_{4,0} \leftarrow 4_{3,1}$  transition:  $\gamma_{0,V}^{Exp} = 4.59(9)$  MHz/mbar,  $\gamma_{0,SDV}^{Exp} = 4.74(3)$  MHz/mbar,  $\gamma_{2,SDV}^{Exp} = 0.66(3)$  MHz/mbar.

(b) N<sub>2</sub>-broadened  $2_{2,1} \leftarrow 2_{1,2}$  transition for  $P_{H_2S} = 0.01$  mbar:  $\gamma_{0,V}^{Exp} = 2.89(2)$  MHz/mbar,  $\gamma_{0,SDV}^{Exp} = 2.941(6)$  MHz/mbar,  $\gamma_{2,SDV}^{Exp} = 0.292(3)$  MHz/mbar. The error bars correspond to one standard deviation (SD); they take into account the different experimental uncertainties: fitting standard deviation (<1%), cell length (0.7%), temperature (0.34%), pressure (0.4%) and the systematic errors linked to detector and electronic nonlinearity (2%).

### 3. Broadening coefficients calculations

#### 3.1. Formalism of the theoretical calculations

Since previous calculations of pressure broadening of H<sub>2</sub>S were performed in the  $\nu_2$  band and for rovibrational lines other than measured in this work, we decided to compute the self- and N<sub>2</sub>-broadening coefficients of H<sub>2</sub>S in the ground vibrational state in order to reproduce our measurements and to detect an eventual vibrational effect on the pressure broadening phenomena. The computations were performed using the semi-classical model based on the RB formalism. Within this formalism, the pressure broadening half-width  $\Gamma_0$  in the unit of **Hz** may be expressed as [39,40,41]:

$$\Gamma_0 = \frac{n}{2\pi} \text{Re} \left[ \sum_{J_2 K_2} \rho_{J_2 K_2} \int_0^{+\infty} v F_{Max}(v) dv \int_{r_{c0}}^{+\infty} 2\pi r_c \left( \frac{v'_c}{v} \right) S(r_c, v) dr_c \right] \quad (10)$$

where  $n$  is the number density of perturbing molecules,  $v$  is the relative velocity between the absorber and the perturber,  $F_{Max}(v)$  is the Maxwell velocity distribution,  $\rho_{J_2 K_2}$  is the relative population of the perturber,  $r_c$  and  $v'_c$  are position and velocity parameters related to the relative trajectories model and  $r_{c0}$  is the distance of closest approach [39]. The differential broadening cross section  $S(r_c, v)$  is given by [40]:

$$S(r_c, v) = 1 - \exp \left( \Re e S_{2,i_2} + \Re e S_{2,f_2} + \Re e S_{2,f_2 i_2} \right) \quad (11)$$

where the  $S_{2,i_2}$ ,  $S_{2,f_2}$  and  $S_{2,f_2 i_2}$  are the second-order terms of the perturbation development of the differential cross section [39,40,42]. To calculate the self- and N<sub>2</sub>-broadening coefficients, we have considered the intermolecular potential involving the electrostatic interactions as well as the induction and the Tipping–Herman potential [43] expressed as:

$$V = V_{\mu_1 \mu_2} + V_{\mu_1 Q_2} + V_{Q_1 \mu_2} + V_{Q_1 Q_2} + 4\epsilon \left[ R_1 \left( \frac{\sigma}{r_c} \right)^{13} - A_1 \left( \frac{\sigma}{r_c} \right)^7 \right] P_1(\cos \theta) + 4\epsilon \left[ R_2 \left( \frac{\sigma}{r_c} \right)^{12} - A_2 \left( \frac{\sigma}{r_c} \right)^6 \right] P_2(\cos \theta) \quad (12)$$

where  $P_1$  and  $P_2$  are the first- and second-order Legendre polynomials,  $\theta$  is the angle between the axis of the absorbing molecule and the intermolecular axis, the indices 1 and 2 refer to the absorber and the perturber,  $\epsilon$  and  $\sigma$  are the Lennard-Jones parameters. In this potential,  $R_1$ ,  $A_1$ ,  $R_2$  and  $A_2$  were chosen to obtain a reasonable agreement with the experimental values of the pressure broadening coefficients. The term due to the electrostatic interactions is a sum of dipole-dipole, dipole-quadrupole, quadrupole-dipole and quadrupole-quadrupole interactions, where  $\mu$  and  $Q$  are the dipole and quadrupole moments of the molecules.

### 3.2. Computations of broadening coefficients

The collisional broadening coefficients of H<sub>2</sub>S self- and -N<sub>2</sub> perturbed have been calculated using the above semiclassical RB formalism with the bi-resonance functions of Starikov [44]. The computation has been performed at the experimental temperature  $T = 296$  K for a complete set of rotational lines. The rotational constants, the electric multipole moments of H<sub>2</sub>S and N<sub>2</sub> and the Lennard-Jones parameters are given in Table 1 with the associated references, as well as the  $A_1$ ,  $R_1$ ,  $A_2$  and  $R_2$  parameters varied manually until obtaining the best agreement between the measured and calculated broadening coefficients.

**Table 1** Molecular parameters used in the calculations of the self- and N<sub>2</sub>-broadening coefficients of H<sub>2</sub>S in the GS.

	H <sub>2</sub> S	N <sub>2</sub>		
$M$ (g.mol <sup>-1</sup> )	34.08	28.0134		
$A$ (cm <sup>-1</sup> )	10.35995 <sup>a</sup>	-		
$B$ (cm <sup>-1</sup> )	9.018496 <sup>a</sup>	1.989622 <sup>d</sup>		
$C$ (cm <sup>-1</sup> )	4.730608 <sup>a</sup>	-		
$\mu$ (D)	0.974 <sup>b</sup>	0		
$Q$ (DÅ)	0.71 <sup>b</sup>	-1.4 <sup>e</sup>		
$\varepsilon$ (K)	309.6 <sup>c</sup>	92.91 <sup>f</sup>		
$\sigma$ (Å)	3.509 <sup>c</sup>	3.816 <sup>f</sup>		
Ajustable parameters				
Molecular system	$A_1$	$R_1$	$A_2$	$R_2$
H <sub>2</sub> S - H <sub>2</sub> S	0.08	1	0.6	0.6
H <sub>2</sub> S - N <sub>2</sub>	0.5	5	0.08	0.08

<sup>a</sup> Ref. [45], <sup>b</sup> Ref. [46], <sup>c</sup> Ref. [47], <sup>d</sup> Ref. [48], <sup>e</sup> Ref. [49], <sup>f</sup> Ref. [50]

## 4. Results and discussion

### 4.1. Self-Broadening coefficients

Table 2 presents the self-broadening coefficients determined from 30 different rotational transitions of H<sub>2</sub>S in the 150 – 850 GHz frequency range with  $0 < J'' < 12$  and  $0 < K_a'' < 8$ . Due to the line narrowing,  $\gamma_{0,SDV}^{Exp}$  should be larger than  $\gamma_{0,V}^{Exp}$ . This assumption is systematically verified with the self-broadening coefficients. The averaged relative variation of the self-

broadening coefficient due to the SD effect  $\frac{\gamma_{0,SDV}^{Exp} - \gamma_{0,V}^{Exp}}{\gamma_{0,V}^{Exp}}$  is estimated to be in the 2% to 12% range with a mean value of about 7.3%. In Table 2 are also reported the  $\frac{\gamma_{2,SDV}^{Exp}}{\gamma_{0,SDV}^{Exp}}$  ratios which give an order of magnitude on speed dependent effects on relaxation. From the mean value of this ratio, about 0.15, and using Eq. (9), one obtains a  $q$  value of about 8.0, which corresponds to a rather hard sphere collision model for the Pickett empirical potential [30]. Table 2 compared also experimental with the calculated self-broadening coefficients using the RB formalism. The mean square difference obtained between the calculated coefficients and the experimental ones adjusted with the Voigt profile is evaluated to 0.34 MHz/mbar. This difference, about 7% the mean value of self H<sub>2</sub>S broadening coefficients, shows the good quality of our theoretical broadening calculations.

In Fig. 4, the experimental and calculated self-broadening coefficients determined in this study are compared with previous measurements in the IR domain for different vibrational bands (Refs. [13,17,14]), and for microwave rotational transitions by Helminger and De Lucia (Ref. [8]). For all these references, the deviation from Voigt profile and the speed dependence effects were not taken into account. The comparison of the different datasets does not allow detect any vibrational dependence. A significant dispersion of the self-broadening coefficient between the different datasets is observed. Tan *et al.* in Ref. [12] have performed a selection of the most reliable self-broadening and air-broadening coefficients of H<sub>2</sub>S for the **HITRAN-2016** edition of the database from different IR datasets [26]. This selection for the self-broadening is also plotted in Fig. 4. From 2016, a first order rotational dependence was considered in the HITRAN database with a linear fit of  $\gamma_{self}$  and  $\gamma_{air}$  versus  $J''+0.2 K_a''$  reproducing the slight decreasing of the broadening coefficients observed in Fig. 4 from  $J''=2$  to  $J''=11$ . For the self-broadening, the mean square difference between the  $\gamma_{0,SDV}^{Exp}$  determined in this study and the values tabulated in **HITRAN-2016** is evaluated to 0.35 MHz/mbar, which is similar to the previous difference between our measurements and RB calculations.

**Table 2.** Self-broadening coefficients of H<sub>2</sub>S in MHz/mbar determined in this study. Frequencies are given in GHz.  $J'$ ,  $K_a'$ ,  $K_c'$ ,  $J''$ ,  $K_a''$ ,  $K_c''$  are the upper and lower state quantum numbers.  $\gamma_{0,V}^{Exp}$ ,  $\gamma_{0,SDV}^{Exp}$  and  $\gamma_{2,SDV}^{Exp}$  are the experimental coefficients fitted with Voigt and SD-Voigt profiles. The ratio  $\frac{\gamma_{2,SDV}^{Exp}}{\gamma_{0,SDV}^{Exp}}$  gives the magnitude of the speed dependence.  $\gamma_{RB}^{Cal}$  are the calculated coefficients with the RB formalism.  $\gamma_{GS}^{Emp}$  are the empirical coefficients based on the Starikov model adjusted with the GS self-broadening coefficients determined in this study (see Section 4). Last digit quoted errors in parentheses are equal to one standard deviation (1 SD).

Frequency	$J'$	$K_a'$	$K_c'$	$J''$	$K_a''$	$K_c''$	$\gamma_{0,V}^{Exp}$	$\gamma_{0,SDV}^{Exp}$	$\gamma_{2,SDV}^{Exp}$	$\frac{\gamma_{2,SDV}^{Exp}}{\gamma_{0,SDV}^{Exp}}$	$\gamma_{RB}^{Cal}$	$\gamma_{GS}^{Emp}$
168.762	1	1	0	1	0	1	4.52(7)	4.84(4)	0.63(2)	0.130(5)	4.61	4.36
216.710	2	2	0	2	1	1	4.91(7)	5.40(2)	0.69(1)	0.128(2)	5.02	5.03
300.505	3	3	0	3	2	1	3.98 (8)	4.34(3)	1.04(2)	0.240(6)	4.80	4.64
369.101	3	2	1	3	1	2	5.39(9)	5.67(3)	1.36(3)	0.240(7)	4.75	5.04
369.127	4	3	1	4	2	2	4.4(1)	4.75(2)	0.74(2)	0.156(5)	4.55	4.66
393.450	2	1	1	2	0	2	5.62(9)	6.08(1)	1.39(6)	0.23(1)	4.99	5.06
407.675	5	4	1	5	3	2	4.08(8)	4.34(2)	0.93(4)	0.21(1)	4.36	4.58
424.314	4	4	0	4	3	1	4.59(9)	4.74(6)	0.66(3)	0.139(8)	4.56	4.47
493.362	6	5	1	6	4	2	4.56(7)	4.74(1)	0.64(2)	0.135(5)	4.17	4.61
505.564	2	2	1	2	1	2	5.09(5)	5.34(1)	1.26(6)	0.24(1)	5.02	5.03
555.254	7	5	2	7	4	3	4.54(9)	4.89(3)	0.84(3)	0.172(7)	4.28	4.54
567.078	6	4	2	6	3	3	4.30 (6)	4.53(2)	0.53(1)	0.117(3)	4.50	4.63
568.049	3	3	1	3	2	2	4.36(7)	4.67(2)	0.93(2)	0.199(5)	4.80	4.64
579.798	5	5	0	5	4	1	4.97(9)	5.15(3)	1.12(3)	0.218(7)	4.33	4.61
593.169	8	6	2	8	5	3	4.17(5)	4.48(3)	0.66(4)	0.15(1)	4.08	4.30
626.473	7	6	1	7	5	2	4.90(9)	5.31(2)	1.19(1)	0.224(3)	3.96	4.46
665.395	4	2	2	4	1	3	5.23(7)	5.60(4)	1.01(5)	0.18(1)	4.96	4.94
687.304	2	0	2	1	1	1	4.01(6)	4.41(3)	0.99(5)	0.23(1)	4.75	4.76
689.121	9	7	2	9	6	3	4.03(9)	4.20(3)	0.52(3)	0.124(8)	3.91	4.05
733.025	10	7	3	10	6	4	4.55(9)	4.90(5)	0.59(3)	0.120(7)	4.03	4.15
746.720	9	6	3	9	5	4	4.34(9)	4.78(2)	0.74(2)	0.155(5)	4.20	4.25
747.301	3	2	2	3	1	3	5.49(8)	5.68 (5)	0.82(3)	0.144(7)	4.75	5.04
748.240	6	6	0	6	5	1	4.44(7)	4.58(3)	0.58(2)	0.127(5)	4.10	4.67
749.433	5	5	1	5	4	2	4.87(6)	5.12(1)	0.71(2)	0.139(4)	4.33	4.61
782.344	11	8	3	11	7	4	4.35(9)	4.79(2)	0.75(4)	0.157(9)	3.91	4.29
794.222	8	7	1	8	6	2	4.54(6)	4.74(4)	0.52(3)	0.110(7)	3.80	4.13
800.850	5	4	2	5	3	3	4.27(5)	4.53(2)	0.68(3)	0.150(7)	4.36	4.58
804.729	8	5	3	8	4	4	4.61(7)	4.80(4)	0.54(2)	0.113(5)	4.39	4.48
839.140	10	8	2	10	7	3	3.64(5)	4.89(3)	0.57(3)	0.117(7)	3.75	3.99
841.280	8	3	6	7	4	3	4.91(6)	5.12(3)	0.83(3)	0.162(7)	4.58	4.51

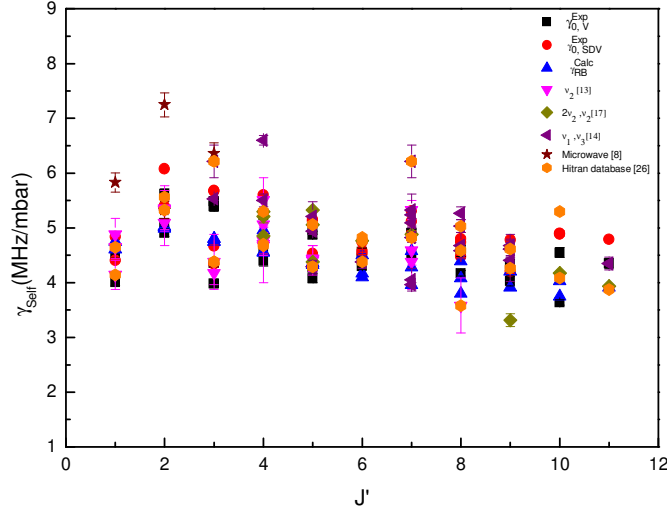


**Fig. 4:** Self-broadening coefficients  $\gamma_{Self}$  determined in this study compared to the previous IR (Refs. [13, 17, 14, 26]) and mw (Ref. [8]) studies.

In order to analyze more finely the rotational dependence of the H<sub>2</sub>S broadening coefficient, the empirical model of Starikov described in Refs. [46,51] for the measured broadening coefficients of C<sub>2v</sub> asymmetric top molecules such as H<sub>2</sub>O and H<sub>2</sub>S was adopted. The self-broadening coefficients for the  $J'_{K'_a, K'_c} \leftarrow J''_{K''_a, K''_c}$  rotational transitions were fitted using the following empirical equation:

$$\gamma(K''_a, K'_a) = \gamma^{Emp} = x_1 + x_2 \frac{\cosh[x_5(K''_a - K'_a)(K''_a + K'_a)]}{\cosh[x_3(K'_a - x_4)] \times \cosh[x_3(K''_a - x_4)]} \quad (13)$$

where the  $J$  rotational dependence is included in an  $x_k$  polynomial function (with  $k = 1, 2, 3, 4$  and 5) given by:

$$x_k = x_{k0} + x_{k1}(J'' + J') + x_{k2}(J'' + J')^2 \quad (14)$$

The parameters  $x_{k0}$ ,  $x_{k1}$ , and  $x_{k2}$  were obtained using a nonlinear least-square method that adjusts the equations (13) and (14) to the experimental values of self-broadening coefficients listed in Table 2 complemented with the calculated values  $\gamma_{RB}^{Cal}$  for the non-measured transitions in the ranges  $0 < J'' < 12$  and  $0 < K''_a < 8$ . These fitted parameters are listed in Table 3 with their uncertainties estimated as the fit standard deviations. These uncertainties do not explicitly reveal the errors from the physical parameters intervening in the experiment, but implicit reflect the accuracy of linewidth measurements. The full set of parameters is included in our GS fit and, contrary to the  $v_2$  fit of Ref. [46], all parameters are determined according to their accuracies.

The  $\gamma_{GS}^{Emp}$  self-broadening coefficients determined in this study from Eq. (13) and Eq. (14) are listed in Table 2. For self-broadening, the comparison between the experimental  $\gamma_{0,V}^{Exp}$  and the empirical  $\gamma_{GS}^{Emp}$  provides a mean square difference evaluated to 0.16 MHz/mbar i.e two times smaller than those obtained with  $\gamma_{RB}^{Cal}$ . This result demonstrates the interest of the empirical modeling of Eq.(13) for the interpolation of unmeasured ( $J,K$ ) lines.

**Table 3:** Parameters adjusted in the Starikov model using Eqs. 13 and 14 for the empirical determination of the self-broadening coefficients.  $x_{1k}$  and  $x_{2k}$  are in unit of  $\text{cm}^{-1}.\text{atm}^{-1}$ ,  $x_{3k}$ ,  $x_{4k}$  and  $x_{5k}$  are unitless. Last digit quoted errors in parentheses are equal to one standard deviation (1 SD).

Parameter	This study (GS)	Ref. [46] ( $\nu_2$ )
$x_{10}$	-5.676(3)	-
$x_{11}$	0.468(3)	0.00275(5)
$x_{12}$	-0.00942(1)	-
$x_{20}$	5.81(4)	0.194(1)
$x_{21}$	-0.45762(5)	-0.00484(7)
$x_{22}$	0.00906(2)	-
$x_{30}$	-0.114(2)	0.107(7)
$x_{31}$	0.01022(2)	0.00306(4)
$x_{32}$	-0.000290(2)	-
$x_{40}$	0.821(4)	5.2(2)
$x_{41}$	0.04542(3)	-0.50(2)
$x_{42}$	-0.03610(3)	0.0215(7)
$x_{50}$	0.0363(4)	0.011(4)
$x_{51}$	0.00194(2)	-
$x_{52}$	-0.0001899(4)	-

The rotational dependences of the self-broadening coefficients in  $K_a''$  and in  $J''$  are presented in Fig. 5 which exhibits significant differences especially at low  $K_a''$  and high  $J$  values with the empirical coefficients adjusted with our SMM measurements and those adjusted with the IR data ( $\nu_2$  band) from Ref. [13]. The increasing of  $\gamma_{0,self}$  with  $J''$  at low  $K_a''$  for the  $^RQ$  sub-branch and the rapid decreasing with  $K_a''$  at high  $J''$  characteristic of the  $\nu_2$  rovibrational transitions are not observed in the present study. In the GS, our  $\gamma_{0,self}$  ( $^RQ$ ) coefficients monotonically decreases with  $K_a''$  and have a weaker variation with  $J''$  at  $K_a''=0$ .

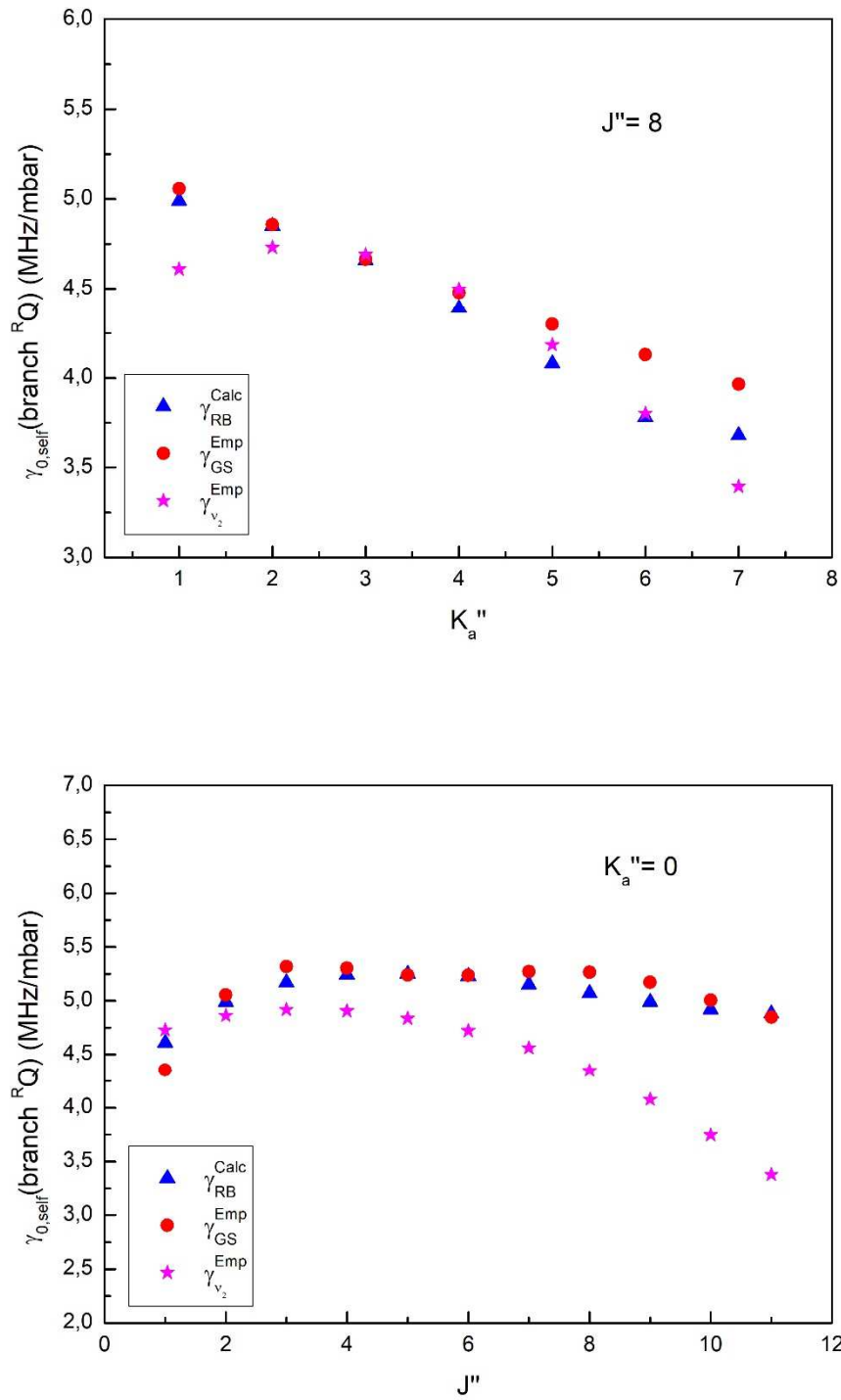


**Fig. 5:** Examples of  $K_a''$  and  $J''$  rotational dependences of the  $\text{H}_2\text{S}$  self-broadening coefficients:  $K_a''$  dependence for  $J''=8$  (top) and  $J''$  dependence for  $K_a''=0$  (bottom). 3 sets of data are compared: the calculated coefficients with the RB formalism  $\gamma_{RB}^{Calc}$  and the empirical coefficients  $\gamma_{GS}^{Emp}$  and  $\gamma_{v_2}^{Emp}$  adjusted respectively on the GS rotational transitions (this study) and the  $v_2$  rovibrational transitions from Ref. [13].

#### 4.2. N<sub>2</sub>-Broadening coefficients

The N<sub>2</sub>-broadening coefficients measured for 27 rotational transitions of H<sub>2</sub>S in the GS with  $0 < J'' < 12$  and  $0 < K_a'' < 8$  using the frequency modulated spectrometer in the frequency range 350 – 810 GHz are listed in Table 4. As for the self-broadening, the SD-Voigt profile provides the best adjustments of the N<sub>2</sub>-broadened rotational lines. The  $\gamma_{0,SDV}^{Exp}$  N<sub>2</sub>-broadening coefficients are greater than the  $\gamma_{0,V}^{Exp}$  coefficients for 70% of the measured lines. In Table 4 are also reported the ratios  $\frac{\gamma_{2,SDV}^{Exp}}{\gamma_{0,SDV}^{Exp}}$  which give an order of magnitude of speed dependent effects on relaxation. From the mean value of this ratio, about 0.10, and using Eq. (9), one obtains a  $q$  value of about 6.0 for the Pickett empirical potential [30], which corresponds approximately to a **Van der Waals** model, revealing lower speed dependent effects than for the self-broadening.

Table 4 present the calculated N<sub>2</sub>-broadening coefficients with the Voigt and SD-Voigt profiles, the adjusted ones and the calculated values using the RB formalism. The mean square difference between  $\gamma_{0,V}^{Exp}$  and  $\gamma_{RB}^{Cal}$  is evaluated to 0.2 MHz/mbar, that about 8% of the mean value of H<sub>2</sub>S-N<sub>2</sub> broadening coefficients. The figure 6 presents the experimental and calculated N<sub>2</sub>-broadening coefficients for all rotational transitions studied in this work compared with previous rotational GS (Ref. [9]) and IR rovibrational measurements in the fundamentals bands  $\nu_1$ ,  $\nu_2$  and  $\nu_3$  (Refs. [15,52]). In these previous studies, only the Voigt profile was used. All datasets exhibit a monotonic decreasing of the N<sub>2</sub>-broadening coefficients with  $J''$  but no vibrational dependence could be unambiguously extracted.

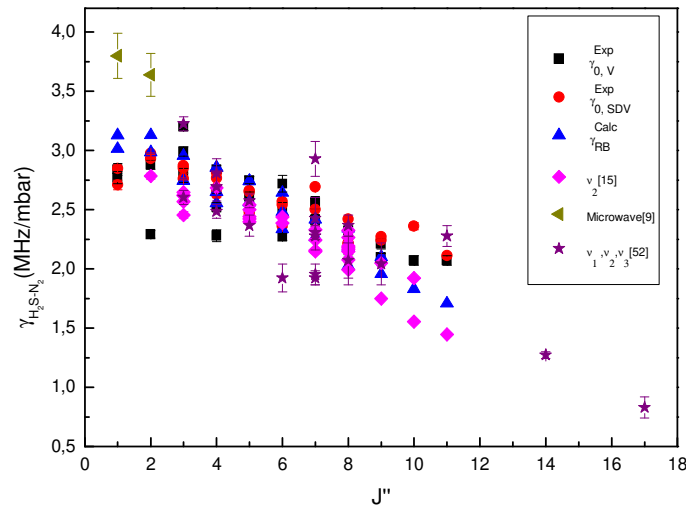


**Fig. 6:** N<sub>2</sub>-broadening coefficients determined in this study compared to the previous IR (Ref. [15, 52]) and MW (Ref. [9]) studies.

**Table 4.** N<sub>2</sub>-broadening coefficients of H<sub>2</sub>S in MHz/mbar determined in this study. Frequencies are given in GHz.  $\gamma_{0,V}^{Exp}$ ,  $\gamma_{0,SDV}^{Exp}$  and  $\gamma_{2,SDV}^{Exp}$  are the experimental coefficients fitted with Voigt and SD-Voigt profiles. The ratio  $\frac{\gamma_{2,SDV}^{Exp}}{\gamma_{0,SDV}^{Exp}}$  gives the magnitude of the speed dependence.  $\gamma_{RB}^{Cal}$  are the calculated coefficients with the RB formalism.  $\gamma_{GS}^{Emp}$  are the empirical coefficients based on the Starikov model adjusted with the GS self-broadening coefficients determined in this study (see Section 4). Last digit quoted errors in parentheses are equal to one standard deviation (1 SD).

Frequency	$J'$	$K_a'$	$K_c'$	$J''$	$K_a''$	$K_c''$	$\gamma_{0,V}^{Exp}$	$\gamma_{0,SDV}^{Exp}$	$\gamma_{2,SDV}^{Exp}$	$\frac{\gamma_{2,SDV}^{Exp}}{\gamma_{0,SDV}^{Exp}}$	$\gamma_{RB}^{Cal}$	$\gamma_{GS}^{Emp}$
369.101	3	2	1	3	1	2	2.99(4)	2.87 (1)	0.24 (1)	0.084(4)	2.75	2.81
369.127	4	3	1	4	2	2	2.81(5)	2.809 (6)	0.266(4)	0.095(2)	2.65	2.66
393.450	2	1	1	2	0	2	3.05(5)	2.972(6)	0.256(3)	0.086(1)	2.99	2.71
407.675	5	4	1	5	3	2	2.75(3)	2.65(2)	0.213(6)	0.080(3)	2.56	2.52
424.314	4	4	0	4	3	1	2.84(3)	2.68(1)	0.197(4)	0.074(2)	2.86	2.74
493.362	6	5	1	6	4	2	2.72(7)	2.57(2)	0.263(9)	0.102(4)	2.48	2.51
505.564	2	2	1	2	1	2	2.89(4)	2.941 (6)	0.292(3)	0.099(1)	3.13	2.79
555.254	7	5	2	7	4	3	2.41(5)	2.50(1)	0.27(2)	0.108(8)	2.27	2.35
567.078	6	4	2	6	3	3	2.50(6)	2.54(1)	0.23(1)	0.091(4)	2.34	2.39
568.049	3	3	1	3	2	2	2.79(6)	2.85(4)	0.25(2)	0.088(8)	2.95	2.89
579.798	5	5	0	5	4	1	2.46(5)	2.45(1)	0.29(2)	0.118(9)	2.74	2.63
593.169	8	6	2	8	5	3	2.32(4)	2.42 (1)	0.267(9)	0.110(4)	2.19	2.22
626.473	7	6	1	7	5	2	2.56(5)	2.690(8)	0.43(4)	0.16(2)	2.42	2.51
650.376	4	4	1	4	3	2	2.52(4)	2.63(4)	0.18(2)	0.068(9)	2.86	2.74
665.395	4	2	2	4	1	3	2.67(3)	2.766(3)	0.237(2)	0.0857(8)	2.56	2.60
687.304	2	0	2	1	1	1	2.77(5)	2.847(7)	0.24(1)	0.084(4)	3.13	2.72
689.121	9	7	2	9	6	3	2.10(3)	2.240(9)	0.19(1)	0.085(5)	2.10	2.07
733.025	10	7	3	10	6	4	2.07(4)	2.36(3)	0.31(3)	0.13(1)	1.83	1.92
736.033	2	1	2	1	0	1	2.84(5)	2.71(4)	0.208(6)	0.077(3)	3.01	2.72
746.72	9	6	3	9	5	4	2.21(4)	2.27(2)	0.246(1)	0.108(1)	1.96	1.96
747.301	3	2	2	3	1	3	3.20(3)	2.760(9)	0.224(1)	0.0812(6)	2.75	2.81
748.240	6	6	0	6	5	1	2.27(3)	2.36(1)	0.162(4)	0.069(2)	2.64	2.67
749.433	5	5	1	5	4	2	2.47(2)	2.478(8)	0.174(5)	0.070(2)	2.74	2.63
782.344	11	8	3	11	7	4	2.07(4)	2.11(2)	0.189(9)	0.090(5)	1.71	1.94
794.222	8	7	1	8	6	2	2.17(5)	2.21(4)	0.139(3)	0.063(3)	2.34	2.39
800.850	5	4	2	5	3	3	2.61(4)	2.66(2)	0.18 (1)	0.068(4)	2.56	2.52
804.729	8	5	3	8	4	4	2.32(5)	2.220(9)	0.158(9)	0.071(4)	2.03	2.10

The N<sub>2</sub>-broadening coefficients were also determined using the empirical model of Starikov (Eqs. (12) and (13)) with the same method applied to the self-broadening. The best parameters determined from the fit of our GS N<sub>2</sub>-broadening coefficients are listed in Table 5 with the parameters obtained in Ref. [46] with the coefficients measured in the v<sub>2</sub> band [15]. In our study, the full set of  $x_k$  parameters was adjusted and correctly determined contrary to those of Ref. [46] where some parameters were not include in the fit (e.g  $x_{11}$ ) and some parameters were not correctly determined (e.g  $x_{30}$  and  $x_{41}$ ). The empirical N<sub>2</sub>-broadening coefficients determined from our  $x_k$  set of parameters are shown in Table 4 (column  $\gamma_{GS}^{Emp}$ ). For N<sub>2</sub>-broadening, the mean square difference between  $\gamma_{0,v}^{Exp}$  and  $\gamma_{GS}^{Emp}$  is evaluated to 0.13 MHz/mbar. As for the self-broadening, this difference is significantly reduced compared to those obtained with the  $\gamma_{RB}^{Cal}$  calculated coefficients.

**Table 5.** Parameters adjusted with the Starikov model (Eqs. (12) and (13)) for the empirical determination of the N<sub>2</sub>-broadening coefficients.  $x_{1k}$  and  $x_{2k}$  are in unit of cm<sup>-1</sup>.atm<sup>-1</sup>,  $x_{3k}$ ,  $x_{4k}$  and  $x_{5k}$  are unitless. Quoted errors in parentheses are in the last digit given and are equal to one standard deviation (1 SD).

Parameter	This study (GS)	Ref. [46] (v <sub>2</sub> )
$x_{10}$	-0.10262(2)	-
$x_{11}$	0.01778(4)	-
$x_{12}$	-0.000505732(3)	-
$x_{20}$	0.21667(4)	0.096(2)
$x_{21}$	-0.02119(2)	-0.0014(2)
$x_{22}$	0.0005253(2)	-
$x_{30}$	0.04042(3)	0.1 (4)
$x_{31}$	-0.00496(2)	-0.0007(2)
$x_{32}$	0.00014697(3)	-
$x_{40}$	-6.499(4)	-1.32(8)
$x_{41}$	9.688(2)	0.3(4)
$x_{42}$	-1.2698(1)	-
$x_{50}$	-0.061(2)	-0.016(2)
$x_{51}$	0.0047421(7)	0.00096(7)
$x_{52}$	-0.00052909(5)	-

The rotational dependences of the N<sub>2</sub>-broadening coefficients on  $K_a''$  and on  $J''$  are presented in Fig. 7. Compared to the self-broadening case (see Fig. 5), the differences between  $\gamma_{GS}^{Emp}$  determined in this study and  $\gamma_{v_2}^{Emp}$  are less pronounced especially for the dependence on  $J''$ .

We can notice that for the N<sub>2</sub>-broadening, the rotational dependence is more significant on  $J''$  than on  $K_a''$  where a roughly linear decreasing of  $\gamma_{0,H_2S-N_2}$  for the <sup>R</sup>Q sub-branch is observed in agreement with previous studies shown in Fig. 6 and the air-broadening rotational dependence associated with the tabulated HITRAN-2016 parameters [12, 26].

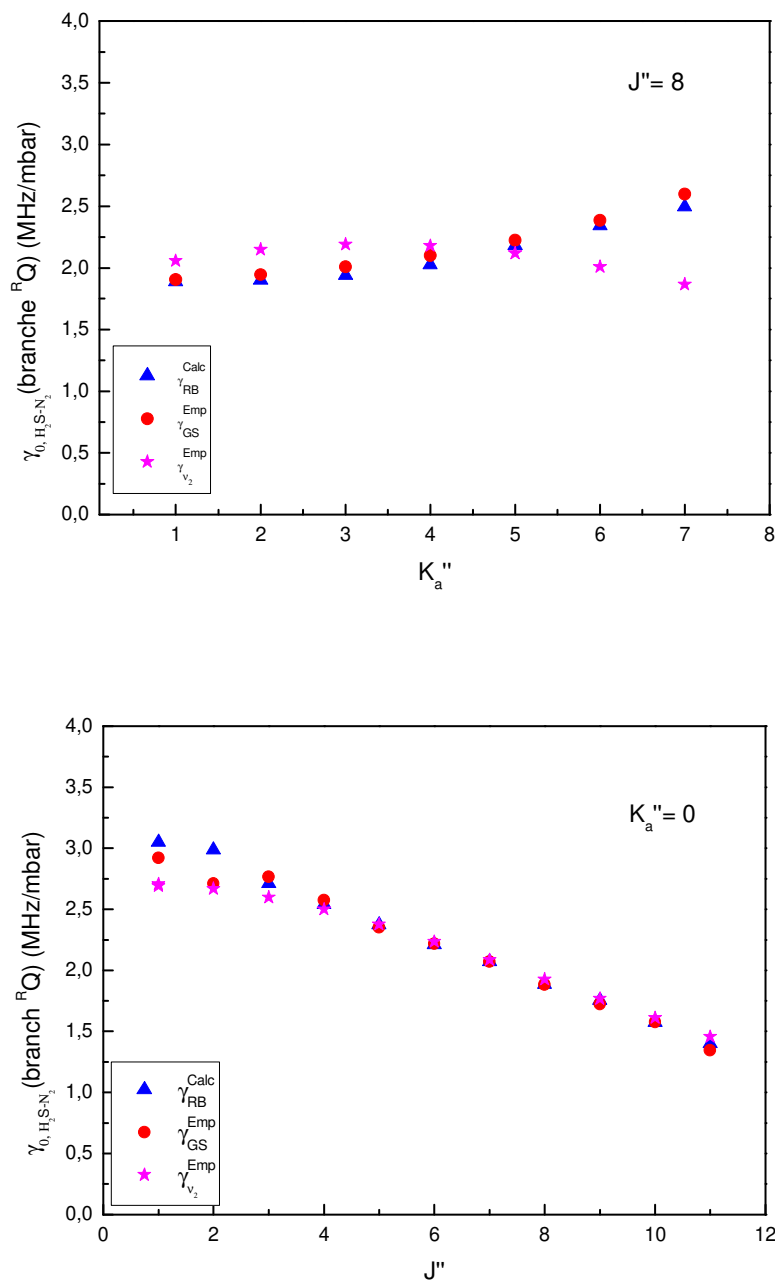


**Fig. 7** Examples of  $K_a''$  and  $J''$  rotational dependences of the H<sub>2</sub>S N<sub>2</sub>-broadening coefficients:  $K_a''$  dependence for  $J''=8$  (top) and  $J''$  dependence for  $K_a''=0$  (bottom). 3 sets of data are compared: the calculated coefficients with the RB formalism  $\gamma_{RB}^{Calc}$  and the empirical coefficients  $\gamma_{GS}^{Emp}$  and  $\gamma_{v_2}^{Emp}$  adjusted respectively on the GS rotational transitions (this study) and on the  $v_2$  rovibrational transitions from Ref. [15].

## 5. Conclusion

With the use of a frequency modulated THz spectrometer and of a dedicated fitting procedure, we have measured, in the 150 – 850 GHz frequency range, a new set of precise self- and N<sub>2</sub>-broadening coefficients at  $T = 295$  K for 30 and 27 GS rotational lines (mainly in the <sup>R</sup>Q sub-branch) of H<sub>2</sub>S, respectively. Benefiting from good S/N ratios (S/N>500) of the measured smm lines, systematic departures from the usual Voigt model have been stated for all the rotational lines studied in this work. The SD-Voigt profile yields to the best residuals and linear pressure dependences of the broadening and speed dependence parameters are observed in the 0.1 – 0.8 mbar pressure range. In addition, the prediction of self- and N<sub>2</sub>-broadening coefficients using the RB formalism with bi-resonance functions leads to a reasonable agreement with the measured values and reproduces the observed rotational dependencies. The experimental broadenings show general consistency with the IR rovibrational measurements performed by other authors, with no evidence of systematic differences between the vibrational states. Using an empirical model developed by Starikov [46, 51] and tested on H<sub>2</sub>S broadening coefficients determined in the  $\nu_2$  fundamental band, the rotational dependences in  $J''$  and  $K_a''$  were analyzed with the self- and N<sub>2</sub>-broadening coefficients measured in this study. Some differences are observed compared to the IR results: (i) our  $\gamma_{0,\text{self}}^{\text{RQ}}$  coefficients monotonically decreases with  $K_a''$  and have a weaker variation with  $J''$  at  $K_a'' = 0$ ; (ii) for the N<sub>2</sub>-broadening, the rotational dependence is more significant on  $J''$  than on  $K_a''$  with a roughly linear decreasing of  $\gamma_{N_2}$  in the <sup>R</sup>Q branch.

The present release of HITRAN does not account for branch and band type interactions, Dicke narrowing, speed dependence effects or line mixing. Such fine effects may be quantified in pure rotation provided sufficient SNR is available. In the case of line mixing higher pressures measurements are required and a specific baseline treatment. Our results suggest that the existing data base information may be extended with some confidence to the H<sub>2</sub>S rotational measurements considered in this work. To go further in this study, it will be interesting to introduce speed-dependent collisional parameters in the semi-classical calculations [53].

## Acknowledgements

This study was undertaken as part of the Terafood project, which is financially supported by the European Regional Development Fund and the province Oost-Vlaanderen (1.2.11). It was also supported by the CaPPA project (Chemical and Physical Properties of the Atmosphere) and CPER-ClimiBio that are funded by the French National Research Agency (ANR) through the

PIA (Programme d'Investissement d'Avenir) under contract "ANR-11-LABX-0005-01", by the Regional Council "Nord-Pas de Calais" and by the "European Funds for Regional Economic Development" (FEDER).

## References

- [1] Hindle F, Kuuliali L, Mouelhi M, Cuisset A, Bray C, Vanwolleghem M, Devlieghere F, Mouret G, Bocquet R. Monitoring of food spoilage by high resolution THz analysis. *Analyst* 2018;143:5536–44.
- [2] Lieven C, Coheur P. F, Chefdeville S, Lacour J. L, Hurtmans D, Clerbaux C. Infrared satellite observations of hydrogen sulfide in the volcanic plume of the August 2008 Kasatochi eruption. *Geophys. Res. Lett.* 2011;38(10):L10804.
- [3] Zahnle K, Marley M. S, Freedman R. S, Lodders K, Fortney J. J, Atmospheric Sulfur Photochemistry on Hot Jupiters. *Astrophys. J. Lett.* 2009;701:20-24.
- [4] Irwin P. G. J, Toledo D, Garland R, Teanby N. A, Fletcher L. N, Orton G. S, Bézard B. Probable detection of hydrogen sulphide (H<sub>2</sub>S) in Neptune's atmosphere. *Icarus* 2019;321:550-63.
- [5] Privalov, V.E, Shemanin V.G. Hydrogen Sulfide Molecules Lidar Sensing in the Atmosphere. *Opt. Mem. Neural Networks* 2018;27:120-31.
- [6] Belov P. S, Yamada K. M. T, Winnewisser G, Poteau L, Bocquet R, Demaison J, Polyansky O, Tretyakov M. Y, Terahertz rotational spectrum of H<sub>2</sub>S. *J. Mol. Spectrosc.* 1995;173:380-90.
- [7] Flaud J. M, Camy-Peret C, Johns J. W. C. The far-infrared spectrum of hydrogen sulfide. The (000) rotational constants of H<sub>2</sub><sup>32</sup>S, H<sub>2</sub><sup>33</sup>S and H<sub>2</sub><sup>34</sup>S. *Can. J. Phys.* 1983;61:1462-73.
- [8] Helminger P, De Lucia F. C. Pressure broadening of hydrogen sulfide. *J. Quant. Spectrosc. Radiat. Trans.* 1977;17:751-54.
- [9] Ball C. D, Dutta J. M, Beaky M. M, Goyette T. M, De Lucia F. C. Variable-temperature pressure broadening of H<sub>2</sub>S by O<sub>2</sub> and N<sub>2</sub>. *J. Quant. Spectrosc. Radiat. Transf.* 1999;61:775–80.
- [10] Minghe L, Swearer D. F, Gottheim S, Phillips D. J, Simmons Jr J. G, Halas N. J, Everitt H. O. Quantitative analysis of gas phase molecular constituents using frequency-modulated rotational spectroscopy. *Rev. Sci. Instrum.* 2019;90:053110-1-13.
- [11] Tasinato N, Pietropolli Charmet A, Stoppa P, Buffa G, Puzzarini C. A complete listing of sulfur dioxide self-broadening coefficients for atmospheric applications by coupling infrared and microwave spectroscopy to semiclassical calculations. *J. Quant. Spectrosc. Radiat. Trans.* 2013;130:233-48.
- [12] Tan Y, Kochanov R.V, Rothman L.S, Gordon I.E. The broadening coefficients of H<sub>2</sub>S (2016), 10.5281/zenodo.34538.
- [13] Waschull J, Kuhnemann F, Sumpf B. Self-, Air, and Helium Broadening in the  $\nu_2$  Band of H<sub>2</sub>S. *J. Mol. Spectrosc.* 1994;165:150–58.
- [14] Sumpf B, Meusel I, Kronfeldt H. -D. Self- and Air-Broadening in the  $\nu_1$  and  $\nu_3$  bands of H<sub>2</sub>S. *J. Mol. Spectrosc.* 1996;177:143–45.
- [15] Kissel A, Sumpf B, Kronfeldt H. -D, Tikhomirov B, Ponomarev Y. Molecular-Gas-Pressure-Induced Line-Shift and Line-Broadening in the  $\nu_2$ -Band of H<sub>2</sub>S. *J. Mol. Spectrosc.* 2002;216:345–54.
- [16] Ciaffoni L, Cummings B. L, Denzer W, Peverall R, Procter S. R, Ritchie G. A. D. Line strength and collisional broadening studies of hydrogen sulphide in the 1.58  $\mu\text{m}$  region using diode laser spectroscopy. *Appl. Phys. B* 2008;92:627–33.
- [17] Sumpf B. Experimental Investigation of the Self-Broadening Coefficients in the  $\nu_1 + \nu_3$  band of SO<sub>2</sub> and the  $2\nu_2$  band of H<sub>2</sub>S. *J. Mol. Spectrosc.* 1997;181:160–67.
- [18] Tran H, Ngo N. H, Hartmann J. M. Efficient computation of some speed-dependent isolated line profiles. *J. Quant. Spectrosc. Radiat. Transf.* 2013;129:199-203.

- [19] Scherbakov A. P, Horneman V. -M, Sydow C, Maul C, Bauerecker S. Extended analysis of the high resolution FTIR spectra of H<sub>2</sub>MS ( $M = 32, 33, 34, 36$ ) in the region of the bending fundamental band: the  $\nu_2$  and  $2\nu_2 - \nu_2$  bands: line positions, strengths, and pressure broadening widths. *J. Quant. Spectrosc. Radiat. Transf.* 2018;216:76-98.
- [20] Mouret G, Guinet M, Cuisset A, Croizé L, Eliet S, Bocquet R, Hindle F. Versatile Sub-THz Spectrometer for Trace Gas Analysis. *IEEE Sensors Journal* 2013;13:133-38.
- [21] Rohart F, Mejri S, Sow P. L.T, Tokunaga S.K, Chardonnet C, Darquié B, Dinesan H, Fasci E, Castrillo A, Gianfrani L, Daussy C. Absorption line shape recovery beyond the detection bandwidth limit: application to the precision spectroscopic measurement of the Boltzmann constant. *Phys. Rev. A* 2014;90:042506,1–12.
- [22] Rohart F. Overcoming the detection bandwidth limit in precision spectroscopy: The analytical apparatus function for a stepped frequency scan. *J. Quant. Spectrosc. Radiat. Transf.* 2017;187:490-504.
- [23] Dore L. Using Fast Fourier Transform to compute the line shape of frequency-modulated spectral profiles. *J. Mol. Spectrosc* 2003;221:93-98.
- [24] Buldyreva J, Margulès L, Motiyenko R. A, Rohart F. Speed dependence of CH<sub>3</sub><sup>35</sup>Cl–O<sub>2</sub> line-broadening parameters probed on rotational transitions: Measurements and semi-classical calculations. *J. Quant. Spectrosc. Radiat. Transf.* 2013;130:304-14.
- [25] Dudaryonok A. S, Lavrentieva N. N, Buldyreva J, Margulès L, Motiyenko R. A, Rohart F. Experimental studies, line-shape analysis and semi-empirical calculation of broadening coefficients for CH<sub>3</sub><sup>35</sup>Cl–CO<sub>2</sub> submillimeter transitions. *J. Quant. Spectrosc. Radiat. Transf.* 2014;145:50-56.
- [26] Gordon I. E, Rothman L. S, Hill C, Kochanov R. V, Tan Y, Bernath P. F and al. The HITRAN 2016 molecular spectroscopic database. *J. Quant. Spectrosc. Radiat. Transf.* 2017;203:3-69.
- [27] Hartmann J. M, Boulet C, Robert D. Collisional effects on molecular spectra. Laboratory experiments and models, consequences for applications. Elsevier, Amsterdam, 2008.
- [28] Dicke R. H. The Effect of Collisions upon the Doppler Width of Spectral Lines. *Phys. Rev.* 1953;89:472-73.
- [29] Berman P. R. Speed-dependent collisional width and shift parameters in spectral profiles. *J. Quant. Spectrosc. Radiat. Transf.* 1972;12:1331–42.
- [30] Pickett H. M. Effects of velocity averaging on the shapes of absorption lines. *J. Chem. Phys* 1980;73:6090–4.
- [31] Ciuryło R, Szudy J, Speed-dependent pressure broadening and shift in the soft collision approximation. *J. Quant. Spectrosc. Radiat. Transf.* 1997;57:411–23.
- [32] Galatry L. Simultaneous effect of Doppler and foreign gas broadening on spectral lines. *Phys. Rev.* 1961;122:1218–24.
- [33] Rohart F, Mäder H, Nicolaisen H. W. Speed dependence of rotational relaxation induced by foreign gas collisions: studies on CH<sub>3</sub>F by millimeter wave coherent transients. *J. Chem. Phys.* 1994;101:6475–86.
- [34] Tennyson J, Bernath P. F, Campargue A, Császár A. G, Daumont L and al. Recommended isolated–line profile for representing high–resolution spectroscopic transitions. *Pure Appl. Chem.* 2014;86:1931-43.
- [35] De Vizia M. D, Castrillo A, Fasci E, Moretti L, Rohart F, Gianfrani L. Investigation on speed–dependence of collision parameters in the H<sub>2</sub><sup>18</sup>O near–IR spectrum: The quadratic model versus the hypergeometric one. *Phys. Rev. A* 2012;85:062512,1–8.
- [36] Rohart F, Nguyen L, Buldyreva J, Colmont J. M, Wlodarczak G. Lineshapes of the 172 and 602 GHz rotational transitions of HC<sup>15</sup>N. *J. Mol. Spectrosc.* 2007;246:213–27.
- [37] Abramowitz M, Stegun I. A. Handbook of Mathematical Functions. Dover, New York, 1965.
- [38] D’Eu J. F, Lemoine B, Rohart F. Infrared HCN lineshapes as a test of Galatry and speed–dependent Voigt profiles. *J. Mol. Spectrosc.* 2002;212: 96–110.
- [39] Robert D, Bonamy J. Short range force effects in semiclassical molecular line broadening calculations. *J. Phys.* 1979;40:923-43.

- [40] Leavitt R. P, Korff D. Cutoff-free theory of impact broadening and shifting in microwave and infrared gas spectra. *J. Chem. Phys.* 1981;74:2180-88.
- [41] Buldyreva J, Lavrentieva N, Starikov V. Collisional line broadening and shifting of atmospheric gases. Imperial College Press, London, 2011.
- [42] Tsao C. J, Curnutte B. Line-widths of pressure-broadened spectral lines. *J. Quant. Spectrosc. Radiat. Trans.* 1962;2:41-91.
- [43] Tipping R. H, Herman R. M. Impact theory for the noble gas pressure-induced HCl vibration-rotation and pure rotation line widths –I. *J. Quant. Spectrosc. Radiat. Trans.* 1970;10:881-96.
- [44] Starikov V. I. Bi-Resonance Functions in the Theory of Collisional Broadening of the Spectral Lines of Molecules. *Opt. Spectrosc.* 2012;112:27-36.
- [45] Azzam A. A, Yurchenko S. N, Tennyson J, Drumel M. A. M, Pirali O. Terahertz spectroscopy of hydrogen sulfide. *J. Quant. Spectrosc. Radiat. Trans.* 2013 ;130 : 341-51.
- [46] Starikov V. I, Protasevich A. E. Broadening of absorption lines of the  $\nu_2$  band of the H<sub>2</sub>S molecule by the pressure of atmospheric gases. *Opt. Spectrosc.* 2006;101:523-31.
- [47] Starikov V. I. *J. Computational Methods in Sciences and Engineering.* 10,599,2010.
- [48] Reuter D, Jennings D. E, Brault J. W. The  $\nu=1\leftarrow 0$  quadrupole spectrum of N<sub>2</sub>. *J. Mol. Spectrosc.* 1986; 115: 294-304.
- [49] Gray C. G, Gubbins K. E. *Theory of Molecular Fluids, Vol. I: Fundamentals.* Oxford University Press, New York 1984.
- [50] Bouanich J. P, Blanquet G, Walrand J. Theoretical O<sub>2</sub>- and N<sub>2</sub>-broadening coefficients of CH<sub>3</sub>Cl spectral lines. *J. Mol. Spectrosc.* 1993;161:416-26.
- [51] Starikov V. I, Protasevich A. E. Analytical Representation for Water Vapor Self-Broadening Coefficients. *Opt. Spectrosc.* 2005;98:330-35.
- [52] Meusel I., Sumpf B., Kronfeldt H. D. Nitrogen Broadening of Absorption Lines in the  $\nu_1$ ,  $\nu_2$ , and  $\nu_3$  Bands of H<sub>2</sub>S Determined by Applying an IR Diode Laser Spectrometer. *J. Mol. Spectrosc.* 1997;185:370-73.
- [53] Ngo N. H., Tran H., Gamache R. R. A pure H<sub>2</sub>O isolated line-shape model based on classical molecular dynamics simulations of velocity changes and semi-classical calculations of speed-dependent collisional parameters. *J. Chem. Phys.* 2012;136:154310.